Available online at www.sciencedirect.com

SciVerse ScienceDirect

Ceramics International 38 (2012) 1591–1597

CERAMICS INTERNATIONAL

www.elsevier.com/locate/ceramint

Influence of particle size and aggregation state of alumina on the rheology of a ceramic paste with an organic binder of ethylene–vinyl acetate copolymer and stearic acid

Setsuaki Murakami [a], Kinki Ri [a], Toshio Itoh [a], Noriya Izu [a], Woosuck Shin [a,*], Koji Inukai [b], Yosuke Takahashi [b], Yasunori Ando [b]

[a] *Electroceramics Processing Research Group, National Institute of Advanced Industrial Science and Technology (AIST), 2266-98 Anagahora Shimoshidami Moriyama-ku, Nagoya 463-8560, Japan*

[b] *R&D Center, Noritake Co., Limited, Miyoshi 470-0293, Japan*

Received 20 July 2011; received in revised form 2 September 2011; accepted 24 September 2011
Available online 29 September 2011

Abstract

The flow behavior of ceramic pastes with various alumina powder contents and different particle sizes, L-particles ($D_{ave.}$ = 6.7 μm) and S-particles ($D_{ave.}$ = 0.13 μm), in an organic binder of ethylene–vinyl acetate copolymer and stearic acid was investigated by dynamic viscoelasticity measurements. The rheological properties of ceramic pastes with high powder content over 19 vol% could not be investigated by the rotational method due to the high viscosity, and were analyzed by the oscillation method. Relative dynamic complex viscosities increased with the powder content, and were consistent with the Dougherty–Krieger model for evaluation of the apparent hydrodynamic shape factor (K_H) and the maximum powder content (f_{cr}^v). The f_{cr}^v and K_H of the L-paste were 0.62 and 1.6, and those of the S-paste were 0.59 and 8.2, respectively. It is considered that the L-particles were comparatively well dispersed and S-particles were aggregated in the paste. These analyses agreed with the aggregates of S-particles determined by SEM observations.

Keywords: A. Suspensions; C. Plasticity; D. Al_2O_3; Ceramic forming process

1. Introduction

Ceramic forming processes can produce complex, accurate and three-dimensional shaped ceramics. The forming process has essentially three steps of mixing, molding and sintering; a ceramic paste is prepared by mixing with an organic binder, and the ceramic paste is melted and injected into a die cavity or extruded through the die to form a green body, and the green body is then heat-treated at high temperature to extract the binder and sinter the ceramic body. The ceramic paste should exhibit good flow behavior during the ceramic forming process and a high ceramic content is also required to reduce shrinkage and crack formation during sintering [1,2]. To obtain sintered specimens without cracks and distortions, important process parameters must be considered, such as the particle size of the ceramic, the dispersion of particles in the paste, and viscoelastic properties such as the yield stress and viscosity of the ceramic paste [3].

Prior to the fabrication of a green body, it is essential that these parameters be predicted. The interparticle distance in the organic binder, the maximum powder content, and the apparent hydrodynamic shape during flow can be predicted using the Woodcock and Dougherty–Krieger models.

The interparticle distance of particles h, in the ceramic paste can be calculated using the Woodcock model [4]:

$$h = d_p\left[\left(\frac{1}{3\pi F}+\frac{5}{6}\right)^{0.5}-1\right], \quad (1)$$

where d_p is the particle size and F is the powder particle content. The interparticle distance of small-sized particles is shorter than that of large-sized particles. Therefore, it is considered that it is difficult to fill the space among small-sized particles with binder. Consequently, the viscosity of a paste

* Corresponding author. Tel.: +81 52 736 7107; fax: +81 52 736 7107.
E-mail address: w.shin@aist.go.jp (W. Shin).

0272-8842/$36.00
doi:10.1016/j.ceramint.2011.09.046

with small-sized particles is higher and the maximum powder content is lower than that for a paste with large-sized particles.

The particle behavior in the paste during flow and the maximum powder content (f_{cr}^{v}) of the ceramic paste can be determined using the Dougherty–Krieger model [5–7]:

$$\eta_r = \frac{\eta_S}{\eta_L} = \left(1 - \frac{f^v}{f_{cr}^v}\right)^{-K_H f_{cr}^v}, \quad (2)$$

where η_r is the relative viscosity, η_S and η_L are the viscosities of the ceramic paste and the organic binder, respectively, f^v is the powder content, and K_H is the apparent hydrodynamic shape factor of the particles. The particle behavior in the paste during flow can be predicted from the obtained K_H [7].

The ceramic forming processes of alumina pastes have been widely investigated [8–11]. The flow behavior of pastes has been investigated using a capillary rheometer, where the paste is forced by a piston through a capillary in the capillary rheometer. Shear stress and the shear rate can be determined under conditions of steady flow by measurement of the pressure drop and volumetric flow rate through the capillary, from which the viscosity can then be calculated [2]. The capillary rheometer is a pragmatic approach and enables understanding of the paste behavior during flow through a die. However, in capillary rheometer measurements, the interface between the die and the paste affects the flow behavior, such as the pressure drop and the volumetric flow rate of the paste. Therefore, it is considered that the structure of the paste cannot be analyzed quantitatively.

In contrast, dynamic viscoelasticity measurements obtained using an oscillation rheometer can provide solid and liquid ratios in the linear and nonlinear regions of the paste. The influence of slip can be minimized by this method, due to the application of a small oscillatory deformation to the paste [10,11]. Therefore, the dispersibility of the particles in the paste and the viscoelastic properties of the paste, such as yield stress and viscosity, can be analyzed quantitatively using an oscillation rheometer. There are few reports where viscosities obtained by an oscillation rheometer are fitted with the Dougherty–Krieger model and where the particle behavior in the paste is discussed quantitatively.

In this study, the dispersibility of alumina particles in an organic binder was analyzed quantitatively using dynamic viscoelasticity measurements. Alumina paste consisting of an organic binder of ethylene–vinyl acetate copolymer (EA) and stearic acid was prepared, and the flow behavior of pastes with various alumina powder contents of different particle sizes (0.13 and 6.7 μm) was analyzed using an oscillation rheometer. The maximum powder content in the paste, the influence of particle size on the flow characteristics and the apparent hydrodynamic shape of the particles are discussed.

2. Experimental method

2.1. Preparation of the ceramic paste

Two alumina powders with different average particle sizes of 6.7 μm (large, L) and 0.13 μm (small, S) were used in this study. The powder was confirmed to be α-phase alumina without any second phase by XRD analysis. BET surface area of L-alumina and S-alumina was 0.933 m^2/g and 13.5 m^2/g, respectively. Fig. 1 shows the particle size distributions and morphologies of the L and S alumina powders.

An organic binder consisting of 40 wt% EA (Vinyl acetate content of about 28 wt% and number average molecular weight of 20,000–40,000. Melting point was 71 °C.) and 60 wt% stearic acid (SA, the SA consists of C18 of 69% and C16 of 30%. Melting point was 57–62 °C.) were used. EA and SA were mixed in a beaker at 120 °C for 2 h. The binder and either the L or S alumina powders were mixed at ceramic contents from 11 to 64 vol% using a kneader (PBV-01, Irie Shokai Co., Japan) at 120 °C for 20 min; the pastes are denoted L-*X*vol% and S-*X*vol%.

Torque value change depending on mixing time for S-59vol% at 120 °C was measured. With extending the mixing time the torque value decreased, and 12 min later the torque value became steady. Therefore, in this study the mixing time was decided to be 20 min to prepare the pastes.

The alumina powder of starting material and the fracture surface of the paste were observed using field emission scanning electron microscopy (FE-SEM; JSM-6335FM, Jeol, Japan). For the FE-SEM observations, a thin coating of Pt was deposited on the surface of the alumina or on the fracture surface of the paste.

2.2. Rheological measurements

The temperature dependence of the dynamic complex viscosity of the organic binder (40 wt% EA and 60 wt% SA) was analyzed using a rheometer (MARS-2, Haake, Germany) with a parallel-plate (35 mm diameter) at temperatures from 40 to 100 °C. The gap between the parallel-plate and the bottom of the measurement vessel was set to be 2 mm. After the parallel-plate approached 2 mm, the excess paste squeezed out was trimmed off.

The flow curves of L-19vol% and S-19vol% were measured using a parallel-plate (8 mm diameter) with a gap of 0.5 mm for shear rates from 0.01/s to 10/s at 70 °C. After the parallel-plate approached 0.5 mm, the excess paste squeezed out was trimmed off. Flow curve measurements of pastes with alumina contents over 19 vol% were unsuccessful due to their high viscosity.

Dynamic viscoelasticity was measured by the oscillation method using a parallel-plate (35 mm diameter) with a gap of 2 mm. Storage modulus (G') and loss modulus (G'') were measured at shear stress values from 5 to 20,000 Pa at a frequency of 0.5 Hz at 70 °C, known as stress sweep measurements.

G' and G'' are usually represented as:

$$G* = G' + iG'', \quad (3)$$

where

$$G' = G^* \cos\ \delta, \quad (4)$$

and

$$G'' = G^* \sin\ \delta, \quad (5)$$

when a viscoelastic fluid is characterized by the phase angle $0 < \delta < 90°$. G' is referred to as the elastic or storage modulus, which is a measure of the energy stored during the test, while

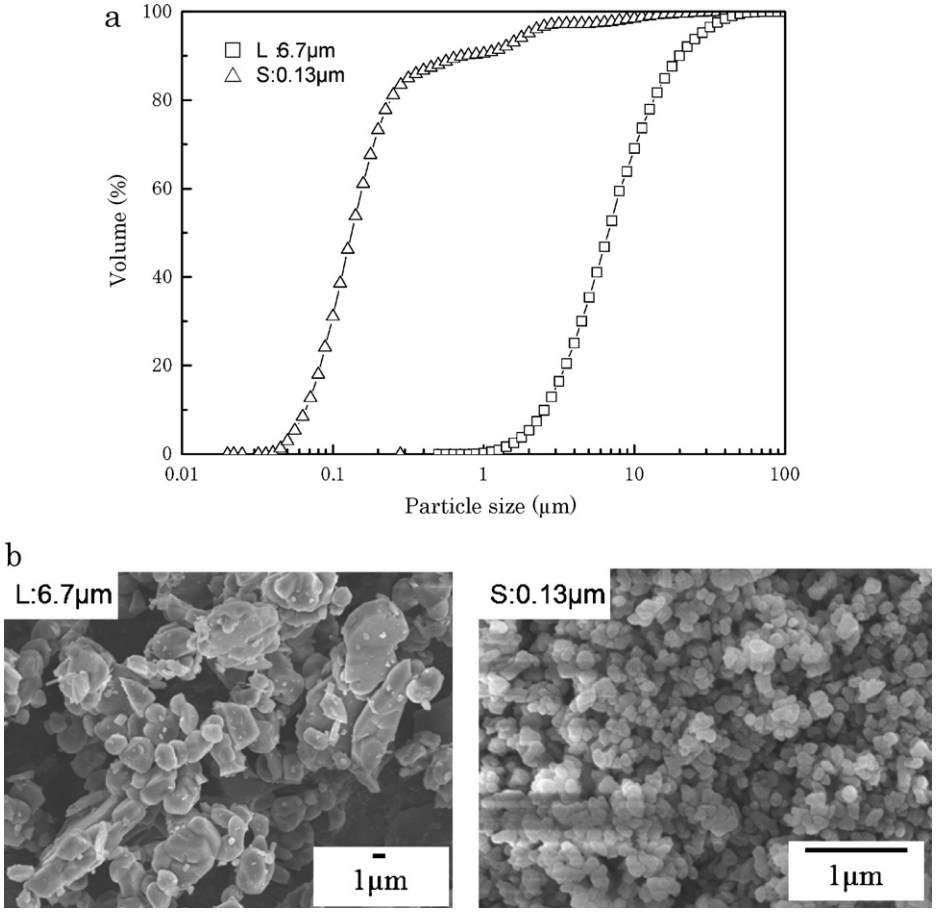

Fig. 1. (a) Particle size distributions and (b) SEM images of two starting alumina powders of L-powder and S-powder.

G'' is the viscous or loss modulus, which is used to determine the energy for flow. In an ideal solid $G^* = G'$, whereas for an ideal liquid $G^* = G''$ [12].

The yield stress of the pastes was obtained from the strain curve of the stress sweep measurement. The inflection point of the strain vs. stress plot with double logarithmic scaling is regarded to be the yield stress.

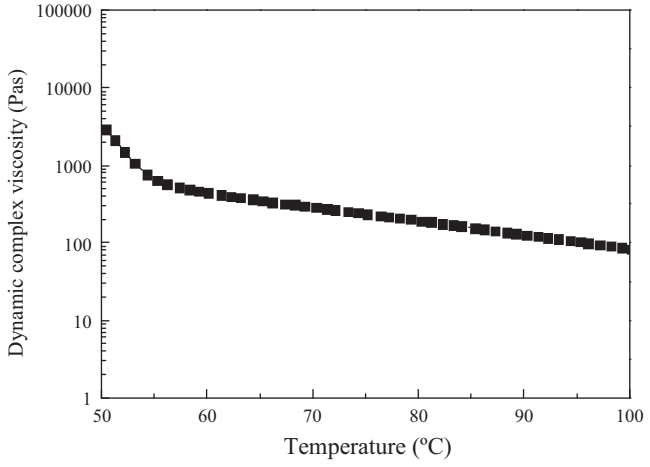

Fig. 2. Temperature dependence of the dynamic complex viscosity of the binder system of ethylene–vinyl acetate copolymer (EA) of 40 wt% and stearic acid (SA) of 60 wt%.

3. Results and discussion

Fig. 2 shows the temperature dependence of the dynamic complex viscosity of the organic binder. G' was lower than G'' for the organic binder at 53 °C, and the organic binder was softened around 53 °C. Upon increase of the temperature, the dynamic complex viscosity of the organic binder decreased. The organic binder composed of EA and SA was thermoplastic. In this study, the paste was analyzed at 70 °C, because of industrial application of ceramic forming at lower temperature.

Hysteresis loops for the shear stress and viscosity of the L-19vol% and S-19vol% pastes were evaluated as a function of shear rate (Fig. 3). The slope of the shear stress curve for L-19vol% was higher than that of S-19vol% and the viscosity of L-19vol% was lower than that of S-19vol%, which indicates that L-19vol% could flow at lower shear stress than S-19vol%. The flow behavior of the paste was affected by the particle size. The loop area in the shear stress plot corresponds to the binding energy of the agglomeration [13], and the loop areas of the L-19vol% and S-19vol% pastes were 11,460 and 52,160 Pa, respectively, which indicates that the S-particles are aggregated in the paste and these aggregates collapse during flow. In contrast, the L-particles were considered to be comparatively well dispersed in the paste.

Fig. 4 shows G' and G'' for L-pastes with various powder contents. G'' for L-pastes with powder contents less than

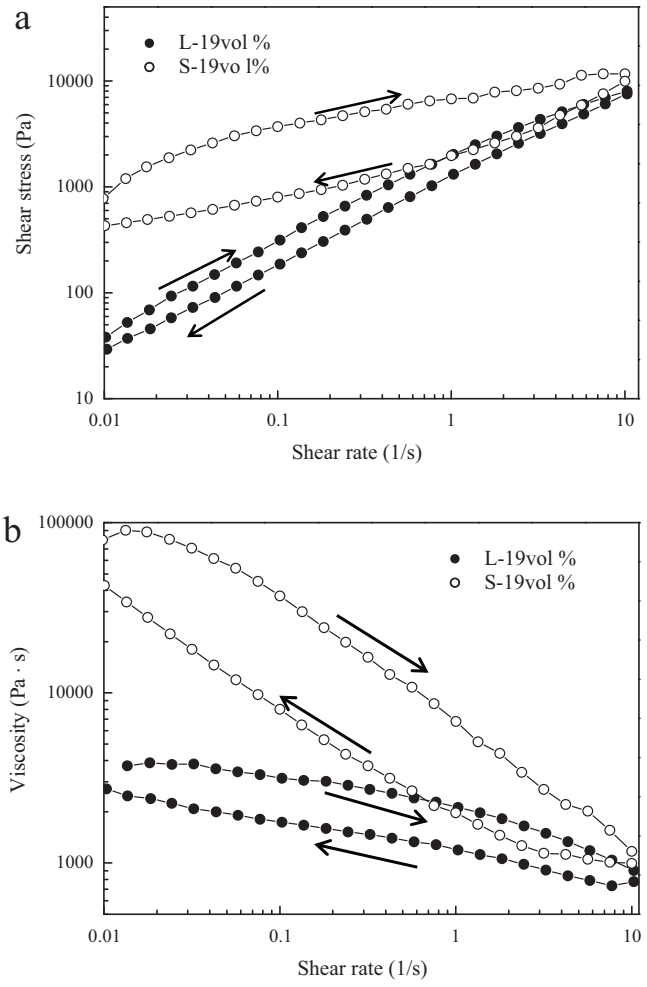

Fig. 3. Hysteresis loop of (a) the shear stress and (b) the viscosity of L-19vol% (●) and S-paste-19vol% (○). L and S indicate the average particle sizes of 6.7 μm and 0.13 μm, respectively.

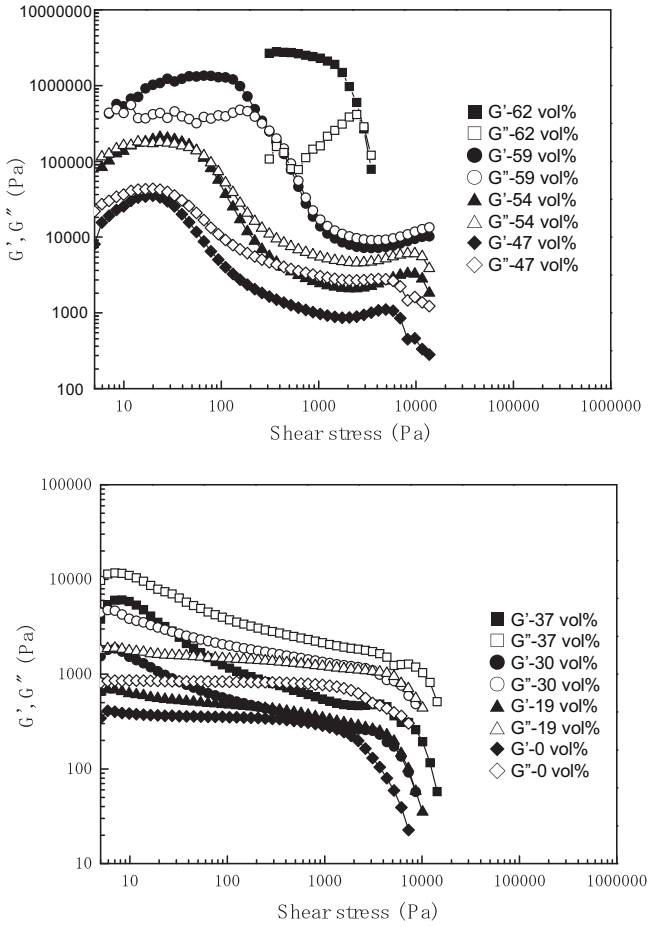

Fig. 4. Shear stress dependence of the storage modulus, G' and the loss modulus, G'' for L-pastes with various powder contents.

47 vol% were higher than G', and these dilute pastes could flow easily at 70 °C. The flow behavior of these pastes was mainly dominated by the organic binder, because of the relationship $G'' > G'$. The abrupt decrease of G' and G'' for pastes with shear stress over 3000 Pa indicates that a slipping layer between the paste and the parallel-plate was created and the parallel-plates slipped. The data over this shear stress region may have an artificial error of slipping. The G' values of the pastes with high powder content over 59 vol% were higher than the G'' values, and the pastes exhibited a cross over. Over the yield stress, G' and G'' crossed over so that G' became lower than G'', and the pastes started to flow. The yield stress data for the pastes and interparticle distance between the particles are summarized in Table 1. The interparticle distances of the particles were calculated according to the Woodcock model (Eq. (1)) [4]. With increasing powder content in the paste, the yield stress increased and the interparticle distance between the particles decreased. Over the yield stress, the paste starts to flow and the particles or the aggregates rotated in the paste.

The L-particles seemed comparatively well dispersed in the paste; however, as the powder content in the paste became high, the interparticle distance decreased and connection of the

Table 1
Yield stress of the paste and interparticle distance values for pastes with different alumina volume fractions.

Average particle diameter (μm)	Particle content (vol%)	Yield stress (Pa)	Interparticle distance (nm)
L: 6.7	0	–	–
	19	–	1205
	30	–	600
	37	7	391
	47	23	195
	54	49	99
	59	110	44
	62	1740	15
	11	50	44
	19	139	23
	30	748	12
S: 0.13	37	2715	8
	47	9727	4
	57	–	1

Yield stress was the bending point of the plot of strain vs. stress in a double logarithmic scaling.
Interparticle distance of the alumina particle was calculated by Woodcock model [4].
"–" in the yield stress indicates no data.

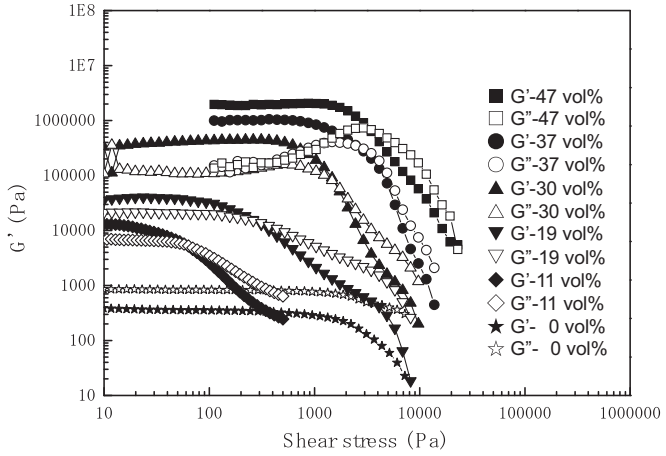

Fig. 5. Shear stress dependence of the storage modulus, G' and the loss modulus, G'' for S-pastes with various powder contents.

particles occurred. Consequently, higher shear stress was necessary to start the flow. L-64vol% collapsed and could not flow, and as a result, the maximum powder content of the L-paste was determined to be 62 vol%.

Fig. 5 shows dependence of G' and G'' for S-pastes with various powder contents. For the S-pastes, G' was a major component ($G' > G''$). Similar to the L-paste, with increase in the powder content, G', G'' and the yield stress (Table 1) increased. Furthermore, upon increasing the shear stress, G' and G'' began to decrease over the yield stress and G'' then prevailed over the cross-over point. S-57vol% and S-59vol% acted as pastes and could flow at 70 °C. However, measurements of G' and G'' for pastes with powder contents over 57 vol% were unsuccessful, because the viscosities of these pastes were very high. The torque of the viscometer was over the measurement range, and consequently the parallel-plates slipped. S-62vol% collapsed and was powder-like, which indicates that the maximum powder content in the S-paste was 59 vol%.

Comparison of the data measured for the L-paste and S-paste with the same particle content of 47 vol% (Fig. 6) indicated that there were more particle aggregates present in the S-paste than

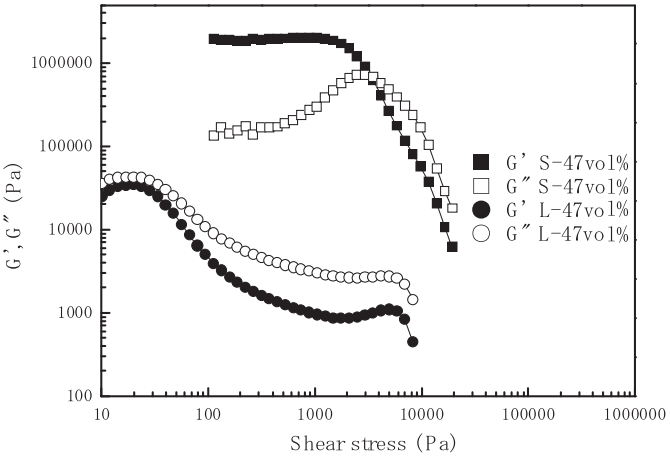

Fig. 6. Shear stress dependence of the storage modulus, G' and the loss modulus, G'' of L-47vol% and S-47vol%. L and S indicate the average particle sizes of 6.7 μm and 0.13 μm, respectively.

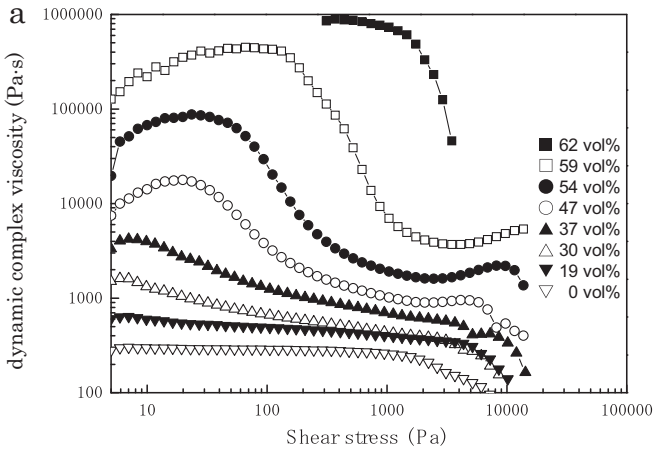

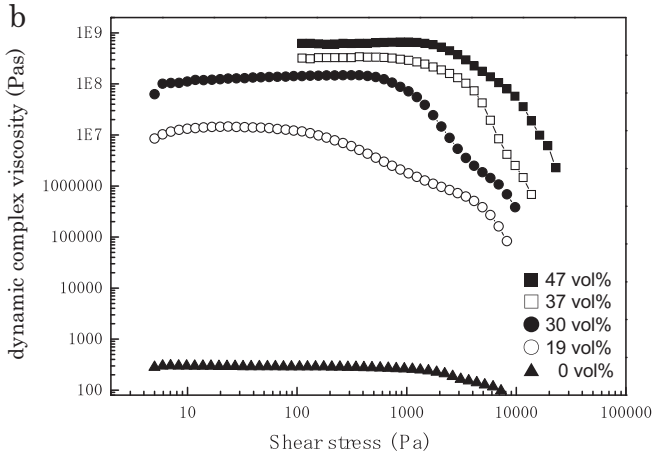

Fig. 7. Relationship between the dynamic complex viscosity of (a) L- and (b) S-pastes with various powder contents and the shear stress. L and S indicate the average particle sizes of 6.7 μm and 0.13 μm, respectively.

in the L-paste, because G' and G'' for the S-paste were over 50 times higher than those for the L-paste. G' prevails over G'' for the S-paste, which suggests that the S-paste is very rigid and solid-like, due to the particle aggregates. The yield stress of L-47vol% was 23 Pa, which is much lower than the 1855 Pa for S-47vol%, as summarized in Table 1. Furthermore, the maximum powder content of the S-paste was 59 vol%, which was lower than that for the L-paste at 62 vol%. The starting material powder with an average particle size of 0.13 μm was aggregated, as shown in Fig. 1b; therefore, it appears that these aggregates in the starting material remained during the mixing of the S-powder and the organic binder with the kneader.

The dynamic complex viscosities of the pastes were fitted using the Dougherty–Krieger model (Eq. (2)) [5–7]. The dynamic complex viscosity was calculated from G', G'' and an angular velocity component. Therefore, the dynamic complex viscosity has viscous and elastic properties, and represents the viscoelasticity of the paste. The decrease of the dynamic complex viscosity around the yield stress indicates the start of flow of a paste.

Fig. 7 shows the relationship between the dynamic complex viscosity of pastes with various powder contents and the shear stress. With increase in the powder content, the dynamic

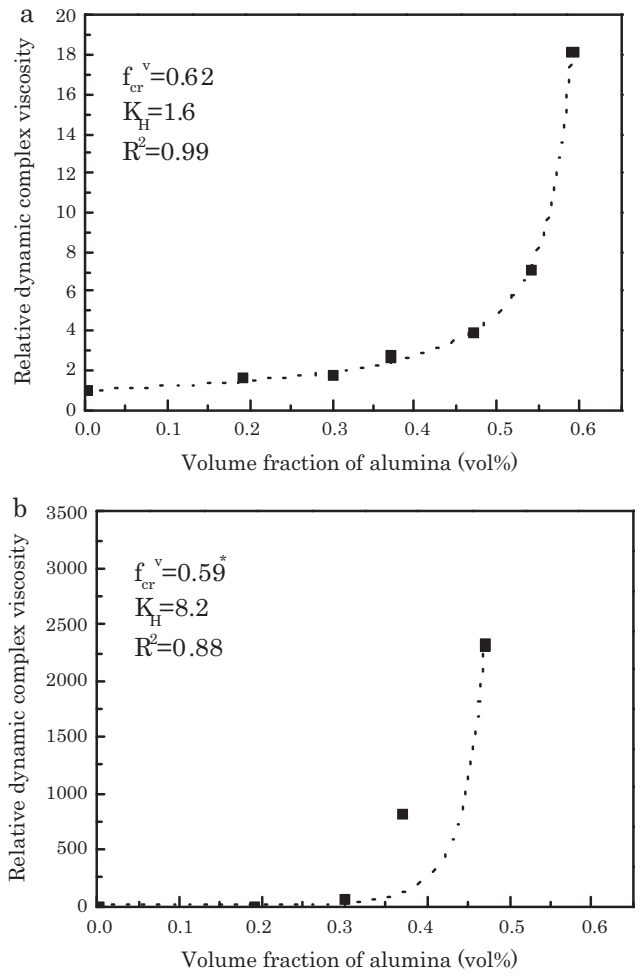

Fig. 8. Relative dynamic complex viscosity (η_S^*/η_L^*) at the shear stress of 2000 Pa with respect to the powder content of (a) L-paste ($D_{ave.}$ = 6.7 μm) and (b) S-paste ($D_{ave.}$ = 0.13 μm). The dotted line represents the fitting curve of Dougherty–Krieger model. f_{cr}^{v*} of the S-paste was fixed to the value of 0.59 which was the upper limit value for the S-paste.

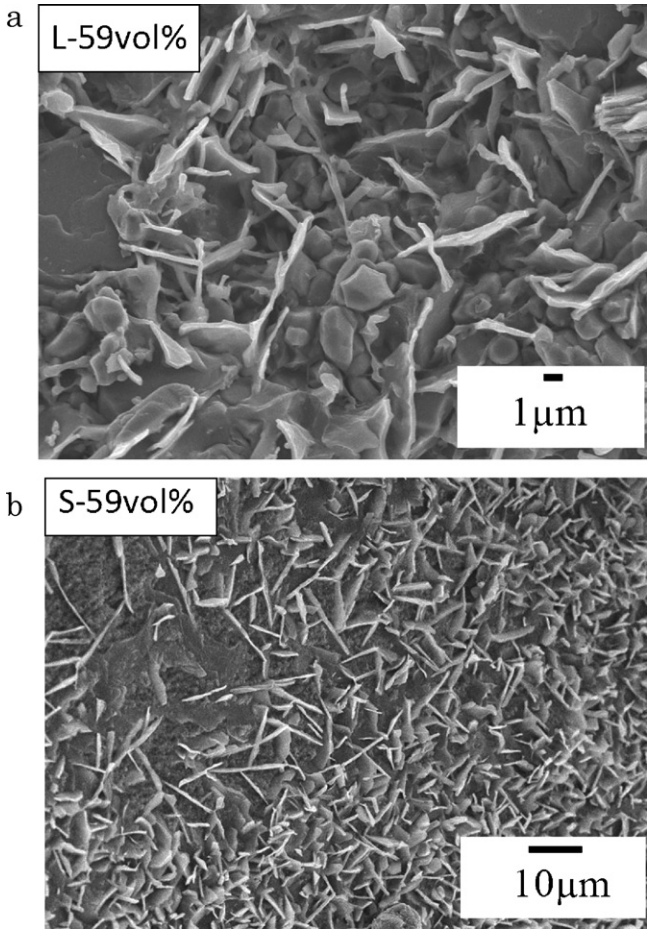

Fig. 9. SEM images of the fractured surface of (a) L-59vol% and (b) S-59vol% pastes. L and S indicated the average particle sizes of 6.7 μm and 0.13 μm, respectively.

complex viscosity of the L- and S-pastes increased and then decreased over the yield stress. The dynamic complex viscosities of the S-paste were higher than those of the L-paste. Similar to the stress sweep measurements (Figs. 4 and 5), measurement of the dynamic complex viscosities over a shear stress of 3000 Pa was unsuccessful for the L- and S-pastes. For the fitting of the Dougherty–Krieger model equation, the dynamic complex viscosities of the pastes at a shear stress of 2000 Pa were used.

Fig. 8 shows the changes in the relative dynamic complex viscosities of the L- (Fig. 8a) and the S-pastes (Fig. 8b) at a shear stress of 2000 Pa, and the dotted line represents the fitting curve of the Dougherty–Krieger model, where K_H is the apparent hydrodynamic shape factor of the particles. For the S-paste, f_{cr}^{v} was fixed at 59 vol%, which was the upper limit value for the paste, because the fitting with the Dougherty–Krieger model failed. At a shear stress of 2000 Pa, K_H and f_{cr}^{v} for the L-paste were 1.6 and 0.62, and that for the S-paste were 8.2 and 0.59, respectively. It has been reported that in pastes with particles having an aspect ratio greater than 1, the particle rotation in the velocity gradient during flow produces a larger effective hydrodynamic volume and $K_H > 2.5$ [7]. In the L-paste, K_H was close in value to 2.5; therefore, it is considered that the L-paste has some aggregates and the spherical shape of these aggregates or of the individual particles rotated during flow. The f_{cr}^{v} of the L-paste was similar to the measured volume of 0.62. For the S-paste, K_H was higher than 2.5 at a shear stress of 2000 Pa; the results of Fig. 3 and the K_H, indicated that the particles in the S-paste were most likely aggregated, which suggests that the aggregates encumbered the flow and rotated in the S-paste during flow. Furthermore, these aggregates were collapsed during flow; therefore, the dispersibility of the S-particles requires enhancement in the paste.

Fig. 9 shows SEM images of the fracture surfaces of the L-59vol% and S-59vol% pastes. The particles in L-59vol% were dispersed between the binder and aggregates of the particles were rarely observed. On the other hand, the particles in S-59vol% were aggregated and the typical size of the aggregates was over 10 μm. These SEM observations were in good agreement with the dynamic viscoelasticity analyses.

Tseng and Teng [14] reported saturation adsorption value of stearic acid on surface of α-alumina with average particle size of 0.25 μm in an organic solvent of toluene was 1.4 mg/m^2.

Using this value an amount of the stearic acid for saturation absorption on L- and S-particle was calculated, and L-62vol% and S-59vol% pastes had the enough amount of stearic acid for the saturation adsorption. However, the SEM photograph of the fracture surface of S-59vol% paste in Fig. 9 shows separation of the binder and the powder phases. It seems that S-alumina particles were not well collapsed by the kneader used in this study and were consequently aggregated in binder system.

In ceramic forming processes, pastes with high powder content and good flow behavior (low yield stress) are desirable for the fabrication of complex-shaped, high-strength ceramic components [2]. The particles in the L-paste were well dispersed; therefore, the L-paste had the higher maximum powder content and better flow properties than the S-paste. However, it is difficult to fabricate micro-complex-shaped ceramic components using the L-paste.

An ideal paste contains well-dispersed small particles without aggregates and has high powder content, good flow behavior and sintering properties. The preparation of a paste containing small particles without aggregates is the most important issue for future investigation. Several considerations, including new organic binders as a dispersant, are under investigation for improved paste preparation.

4. Conclusion

The flow behavior of ceramic pastes with various powder contents and different particle sizes of alumina (6.7 and 0.13 μm) in an organic binder consisting of EA and SA was investigated by dynamic viscoelasticity measurements at 70 °C. The relative dynamic complex viscosities increased with the powder content, and were well fitted by the Dougherty–Krieger model for evaluation of the apparent hydrodynamic shape factor (K_H) and the maximum powder content (f_{cr}^{v}). The dynamic complex viscosities and yield stress of the L- and S-pastes increased with the increase in the powder content. The dynamic complex viscosities and yield stress of the L-pastes were lower than those of the S-pastes. f_{cr}^{v} and K_H for the L- and S-pastes were 0.62 and 1.6, and 0.59 and 8.2, respectively. It is considered that the L-particles were comparatively well dispersed, whereas the S-particles were aggregated in the pastes. The aggregates in the S-paste encumbered the flow and increased the viscosity of the paste. The dynamic viscoelasticity analyses were in good agreement with SEM observations.

References

[1] W.J. Tseng, D.M. Liu, C.K. Hsu, Influence of stearic acid on suspension structure and green micro structure of injection-molded zirconia ceramics, Ceram. Int. 25 (1999) 191–195.
[2] M.E. Sotomayor, A. Varez, B. Levenfeld, Influence of powder particle size distribution on rheological properties of 316L powder injection moulding feedstocks, Powder Technol. 200 (2010) 30–36.
[3] M.J. Edirisinghe, H.M. Shaw, K.L. Tomkins, Flow behaviour of ceramic injection moulding suspensions, Ceram. Int. 18 (1992) 193–200.
[4] H. Kamiya, M. Iijima, Aggregation and dispersion behaviour control of nanoparticles in liquid phase, J. Soc. Powder Technol. Jpn. 46 (2009) 605–614 (in Japanese).
[5] I.M. Krieger, T.J. Dougherty, A mechanism for non-Newtonian flow in suspension of rigid spheres, Trans. Soc. Rheol. 3 (1959) 137–152.
[6] K. Okada, Y. Nagase, Viscosity and powder dispersion in ceramic injection molding mixtures, J. Chem. Eng. Jpn. 33 (2000) 168–173.
[7] J.S. Reed, Rheology of saturated systems (slurries and pastes), in: Principles of Ceramics Processing, second ed., John Wiley and Sons, Inc., 1995, pp. 291–297.
[8] P.T. Vielma, A. Cervera, B. Levenfeld, A. Varez, Production of alumina parts by powder injection molding with a binder system based on high density polyethylene, J. Eur. Ceram. Soc. 28 (2008) 763–771.
[9] W.W. Yang, L.Y. Yang, M.H. Hon, Effects of PEG molecular weights on flow behavior of alumina injection molding feedstocks, Mater. Chem. Phys. 78 (2002) 416–424.
[10] K. Okada, Y. Nagase, Prediction of shear viscosity for ceramic injection molding mixtures, J. Chem. Eng. 33 (2000) 927–929.
[11] B. Loebbecke, R. Knitter, J. Haubelt, Rheological properties of alumina feedstocks for the low-pressure injection moulding process, J. Eur. Ceram. Soc. 29 (2009) 1595–1602.
[12] I. Santacruz, J. Binner, Rheological characterization and coagulation casting of Al_2O_3–nano zirconia suspensions, J. Am. Ceram. Soc. 91 (2008) 33–40.
[13] H.A. Barnes, Thixotropy – a review, J. Non-Newtonian Fluid Mech. 70 (1997) 1–33.
[14] J.W. Tseng, K.H. Teng, The effect of surfactant adsorption on sedimentation behaviors of Al_2O_3–toluene suspensions, Mater. Sci. Eng. A 318 (2001) 102–110.